












# Chitosan-based hydroxylapatite nanostructured membranes containing sodium alendronate for guided bone regeneration therapy

Fábio Luiz Costa de Souza<sup>1</sup> , Alice Simon<sup>1</sup> , Evandro Lúcio Barcelos D'Ornellas<sup>1</sup> , Raphael Ferreira da Silva<sup>1</sup> , Ana Carolina Mattos Covas<sup>1</sup> , Carlos Rangel Rodrigues<sup>1</sup> , Luiz Claudio Rodrigues Pereira da Silva<sup>2</sup> , Flávia Almada do Carmo<sup>1</sup> , Lucio Mendes Cabral<sup>1\*</sup> 

<sup>1</sup>Laboratório de Tecnologia Industrial Farmacêutica (LabTIF), Departamento de Fármacos e Medicamentos, Faculdade de Farmácia, Universidade Federal do Rio de Janeiro—UFRJ, Rio de Janeiro, Brazil.

<sup>2</sup>Laboratório de Nanoteranósticos (LNT), Departamento de Fármacos e Medicamentos, Faculdade de Farmácia, Universidade Federal do Rio de Janeiro—UFRJ, Rio de Janeiro, Brazil.

## ARTICLE INFO

Received on: 02/04/2023  
Accepted on: 09/07/2023  
Available Online: 04/08/2023

### Key words:

Chitosan, guided bone regeneration, hydroxylapatite, membrane, nanocomposite, sodium alendronate.

## ABSTRACT

Guided bone regeneration is commonly applied in clinical dental practice for alveolar bone reconstruction. This work aims to develop nanostructured membranes with chitosan, hydroxylapatite, and sodium alendronate for guided bone regeneration. Low, medium, and high molecular weight chitosan membranes were prepared to contain hydroxylapatite or nanoparticulate hydroxylapatite and sodium alendronate added directly in the polymer matrix or interlayered between clay lamellae. The membranes were analyzed for nanocomposite formation by X-ray diffraction and differential scanning calorimetry analyses, and water absorption and tensile strength were also assessed. *In vitro* assays using Saos-2 cells checked the biocompatibility, cell viability, and osteoinduction potential of the membranes. The chitosan and hydroxylapatite physical mixture membrane series did not form nanocomposites and collapsed in the water absorption test. Membranes with nanoparticulate hydroxylapatite with sodium alendronate interspersed formed nanocomposites and showed a good profile of water absorption and tensile strength. All nanocomposite membranes were biocompatible and demonstrated potential for osteoinduction *in vitro*. The membranes of the nanoparticulate hydroxylapatite series presented the best performance in the *in vitro* assays, especially the membrane formed with low and medium molecular weight chitosan, representing a potential new therapy for guided bone regeneration, which should be tested *in vivo* in the near future.

## INTRODUCTION

Guided tissue regeneration is a technique described in the 1950s when for the first time, a membrane was used as a barrier to separate adjacent tissues from an area with active bone formation in the spine (Wang *et al.*, 2016). The objective of guided

tissue regeneration is the regeneration of bone defects by applying an occlusive membrane that acts as a barrier to the migration of nonosteogenic tissues and, at the same time, as a mechanical support for the growth of bone tissue during its healing process (Kawase *et al.*, 2010; Sheikh *et al.*, 2016). The guided tissue regeneration technique is usually used to regenerate bone tissue around dental implants and is referred to as guided bone regeneration (Dahlin *et al.*, 1989; Wang *et al.*, 2016). Guided bone regeneration is currently one of the most commonly applied methods in clinical dental practice for alveolar bone reconstruction and treatment of peri-implant deficiencies (Lee and Kim, 2014; Wang *et al.*, 2016). Despite autogenous bone grafts being considered the gold standard for bone reconstruction, the only one that presents osteogenesis, osteoinduction, and osteoconduction properties, this

\*Corresponding Author  
Lucio Mendes Cabral, Laboratório de Tecnologia Industrial Farmacêutica (LabTIF), Departamento de Fármacos e Medicamentos, Faculdade de Farmácia, Universidade Federal do Rio de Janeiro—UFRJ, Rio de Janeiro, Brazil.  
E-mail: [lmcabral@pharma.ufrj.br](mailto:lmcabral@pharma.ufrj.br)

technique presents some negative aspects, including the necessity for a second surgical procedure for bone harvesting, a longer operative time, and concerns about donor site morbidity. The risk of complications is increased, such as permanent nerve damage and infections (Betz, 2002; Parvini *et al.*, 2018).

In order to ensure adequate guided bone regeneration, a resorbable and biocompatible membrane is considered ideal, which must present appropriate degradation/resorption times for bone tissue regeneration, appropriate mechanical properties, and support for tissue growth (Basile *et al.*, 2015; Bhowmick *et al.*, 2018; Cao *et al.*, 2017; Shahriarpanah *et al.*, 2016; Sheikh *et al.*, 2016). Resorbable membranes made of collagen and nonresorbable membranes made of polytetrafluoroethylene have been the most commonly used since the introduction of this technique in dental clinical practice (Lee and Kim, 2014; Wang *et al.*, 2016). Despite the various clinical studies available in the literature demonstrating the usefulness of collagen, polytetrafluoroethylene, and resorbable synthetic polymer membranes, they still have limitations related to the characteristics that an ideal membrane for guided bone regeneration should have (Farraro *et al.*, 2014; Lee and Kim, 2014; Wang *et al.*, 2016). Over the years, several other resorbable synthetic materials have been developed, aiming to the creation of a membrane with a good balance between rigidity, elasticity, degradation time, biocompatibility, and good clinical handling—all fundamental requirements for guided bone regeneration success (Giannitelli *et al.*, 2015; Sheikh *et al.*, 2016).

In this context, numerous studies exist on the development of a membrane with ideal characteristics for guided tissue regeneration using the most diverse materials (Lee and Kim, 2014). A new alternative would be the use of silicates such as hydrotalcites [ $\text{Mg}_6\text{Al}_2(\text{CO}_3)(\text{OH})_{16}\cdot 4\text{H}_2\text{O}$ ], which are double lamellar hydroxides containing anionic species in their interlayered domain and that present 2:1 layers, enabling their dispersion (exfoliation) in a polymeric matrix to form nanocomposites (Coelho and Santos, 2007). Bhowmick *et al.* (2018) reported that several studies had demonstrated the positive effect of combining clays and polymers to obtain nanostructured materials with appropriate properties for guided bone regeneration, highlighting the use of chitosan as a polymeric material suitable for this purpose.

Chitosan is a low-cost natural biopolymer that presents biocompatibility, bioadhesiveness, biodegradability, nonimmunogenicity, and nontoxicity and is capable of forming flexible films, in addition to having antimicrobial properties (Bhowmick *et al.*, 2018; Kumar-Krishnan *et al.*, 2015). Moreover, chitosan is structurally similar to some glycosaminoglycans in the bone extracellular matrix, which interact with collagen fibers, and this is the probable reason for its excellent cell adhesion and osteoconductivity properties, one of the reasons why chitosan has been great interest as a material for guided bone regeneration (Logithkumar *et al.*, 2016; Shahriarpanah *et al.*, 2016).

The nanocomposite preparation of chitosan with silicates in nanometric dimensions, interspersed with preserved lamellae or exfoliated by the polymer, can positively affect the derived membranes' mechanical and thermal properties when compared to the use of isolated polymer or its physical mixtures (Huang *et al.*, 2017). Chitosan combined with hydrotalcites can result in four different nanocomposite morphologies, depending on the forces of interaction at the interface between the chitosan and the hydrotalcite lamellae (Kong *et al.*, 2017; Shokuhfar *et al.*, 2012; Zare and Rhee, 2017). The association of a bone resorption

inhibiting drug is extremely advantageous in terms of guided bone regeneration, and sodium alendronate would be one of the drugs of interest in this context (Boanini *et al.*, 2008; Killeen *et al.*, 2012; Pradeep *et al.*, 2013; Ren *et al.*, 2017; Wang *et al.*, 2010; Yun and Kwon, 2006). The potent inhibitory action of sodium alendronate on osteoclast-mediated bone resorption would possibly have an important effect on bone tissue regeneration, especially if it occurred for a prolonged period directly at the defect site. There are no reports in the literature about using sodium alendronate associated with hydrotalcite as a material present in membranes for guided bone regeneration, which could be a promising strategy.

Therefore, the objective of the present work was the development of nanostructured membranes of chitosan and hydrotalcite containing sodium alendronate, aiming for osteoinduction in guided bone regeneration therapy.

## MATERIALS AND METHODS

### Preparation and characterization of nanoparticulate hydrotalcite

The nanomilling process of hydrotalcite ( $[\text{Mg}_6\text{Al}_2(\text{CO}_3)(\text{OH})_{16}\cdot 4\text{H}_2\text{O}]$ ) obtained from Sigma-Aldrich<sup>®</sup>, Merck, Brazil) was carried out in a Netzsch Labtec LB 227/03 ball mill equipped with a 165 ml stainless steel cup and a 30 mm diameter stainless steel unit ball, fixed to a mechanical arm with vertical upward and downward movement with constant speed. The nanomilling was carried out in a dry condition, with the addition of 3 g aliquots of hydrotalcite at a time and a 120-minute nanomilling cycle. The hydrotalcite particles obtained after the nanomilling process were characterized by dynamic light scattering. The average hydrodynamic diameter and polydispersity index (PDI) of hydrotalcite as supplied and after the nanomilling process were determined using a Malvern Zetasizer Nano S90 particle size analyzer (Malvern Instruments, United Kingdom), at 25°C, with a 90° detection angle and He-Ne laser (4 mW) operating at 633 nm. The samples ( $n = 3$ ) were previously prepared by dispersing 0.1% (w/v) of nanoparticulate hydrotalcite in distilled water, containing 0.2% of polysorbate 80, followed by 15 minutes of magnetic stirring at 400 rpm and ultrasonication in a Hielscher UP 100H sonicator, operating at 100% amplitude.

Next, the nanoparticulate hydrotalcites were characterized by X-ray diffraction to confirm that their crystalline domain was not destroyed by the nanomilling process. X-ray diffractometer Shimadzu LABX XRD-6,100 (Kyoto, Japan) was used, operating with a power of 40 kV and current of 30 mA, using  $\text{CuK}\alpha$  radiation as a source of X-ray and a wavelength of 1.542 Å. The diffractometer was adjusted in a parallel beam geometry system, with a divergence slit of 1°, spreading slit of 1°, and reception slit of 0.3 mm. The data were collected in the range of  $2\theta$  between 2° and 85°, with a sampling step of 0.02°, in continuous mode and scanning speed of 2°/minute, at room temperature and atmospheric pressure. Special attention was given to the range of  $2\theta$  between 6° and 30°, corresponding to the hydrotalcite basal reflection, aiming to observe any crystalline structure modification, such as the lamellae exfoliation caused by the nanomilling process.

### Intercalation of sodium alendronate into nanoparticulate hydrotalcite

Nanoparticulate hydrotalcite (0.5 g) was dispersed in 39 ml of distilled water: ethanol 96% (1:1) solution and kept under magnetic stirring (200 rpm) for 30 minutes. In parallel, 1 g of sodium alendronate was solubilized in 37 ml of distilled water

and kept under magnetic stirring (200 rpm) for 30 minutes. The sodium alendronate solution was then added to the nanoparticulate hydroxalcalite dispersion and the system remained under magnetic stirring (200 rpm) and heating in an oil bath at 60°C for 72 hours, after which the mixture was stored under refrigeration at 8°C for 24 hours (Ambrogi *et al.*, 2002; Heraldy *et al.*, 2016).

After 24 hours, the mixture was centrifuged at 19,000 rpm for 30 minutes under refrigeration, after which the supernatant was drained and stored. The precipitate was then resuspended in distilled water and again centrifuged at 19,000 rpm for 60 minutes, after which the supernatant was drained and stored together with the initial supernatant. The cycle of resuspending the precipitate and centrifuging and draining the supernatant was repeated two more times (a total of up to four washing cycles). At the end of the last cycle, both the precipitate and the supernatant recovered were freeze-dried and stored.

The freeze-dried precipitate containing nanoparticulate hydroxalcalite interspersed with sodium alendronate was subjected to analysis by X-ray diffraction to calculate the interlamellar distance of hydroxalcalite using the Bragg equation and was also analyzed using infrared spectroscopy equipment with the Fourier transform Shimadzu IR Prestige-21 (Kyoto, Japan). The freeze-dried supernatant was quantified by gravimetric analysis to determine the sodium alendronate percentage recovered. Gravimetric analysis was performed in triplicate.

#### Obtention of chitosan-based membranes

The membranes were prepared with low (20–300 cP), medium (200–800 cP), or high (800–2,000 cP) molecular weight chitosan (75%–85% deacetylated) (obtained from Sigma-Aldrich®, Merck, Brazil). The chitosan was combined in the proportion 2:1 (polymer: hydroxalcalite) with the following: (1) hydroxalcalite as supplied and sodium alendronate added in the polymer matrix (5% w/w in relation to the polymer mass); (2) nanoparticulate hydroxalcalite and sodium alendronate added in the polymer matrix (5% w/w in relation to the polymer mass); (3) nanoparticulate hydroxalcalite and sodium alendronate interspersed within hydroxalcalite nanoclay lamellae (5% w/w in relation to the polymer mass). All membranes were prepared with 20% (w/w) of glycerin (acquired from Vetec Quimica®, Rio de Janeiro, Brazil) and 10% (w/w) of triacetin (acquired from Multichemie®, São

Paulo, Brazil), with all percentages calculated in relation to the polymer mass (Table 1).

The membranes were prepared according to the casting technique followed by solvent evaporation, as described by Villaça *et al.* (2017). Hydroxalcalite was dispersed in a 1% acetic acid solution containing 5% (w/w) propylene glycol and 0.5% (w/w) polysorbate 80, both relative to the hydroxalcalite products mass, followed by 30 minutes of magnetic stirring at 400 rpm and ultrasonication in a Hielscher UP 100H sonicator, operating at 100% amplitude. Glycerin and triacetin were added to the resultant hydroxalcalite dispersion. Chitosan was dissolved in a 1% acetic acid solution under mechanical stirring, followed by the dissolution of sodium alendronate in the chitosan solution, also under mechanical stirring. The hydroxalcalite dispersion containing glycerin and triacetin was then added to the chitosan and sodium alendronate solution and kept under mechanical stirring (500 rpm), at room temperature, for 3 hours. The resulting mixture was subjected to degassing in an ultrasound bath for 1 hour, poured into glass Petri dishes ( $r = 6$  cm), and stored in an oven at 50°C for 24 hours for solvent evaporation and membrane formation. After drying, the Petri dishes were left for 24 hours at room temperature; then, the membranes were manually removed from the Petri dishes.

Physical mixtures were also prepared for comparison. The preparation of the physical mixtures strictly followed the same procedure adopted for the membranes, except that the mixture of hydroxalcalite dispersion containing glycerin and triacetin and the solution of chitosan and sodium alendronate remained under mechanical stirring for different times, with the mixture requiring only 10 minutes just to homogenize it.

#### Characterization of chitosan-based membranes

All membranes were submitted to X-ray diffraction analysis following the methodology previously described. The membranes obtained were also submitted to differential exploratory calorimetry analysis in Shimadzu DSC-60 equipment (Kyoto, Japan), operated under nitrogen flow of 50 ml/minute in the temperature range of 30°C–350°C and heating rate of 10°C/minute using hermetically sealed aluminum cells.

Membranes were subjected to a dynamic water absorption test to evaluate their swelling properties and estimate the effect of water on their integrity. The dynamic water absorption

**Table 1.** Chitosan-based membranes composition prepared according to the casting technique followed by solvent evaporation.

Membrane code	Membrane component								
	CS-L	CS-M	CS-H	HTC	HTC-N	HTC-N-SA	SA	Glycerin	Triacetin
CS-L:HTC	2.0 g	-	-	1.0 g	-	-	0.1 g	0.4 g	0.2 g
CS-M:HTC	-	2.0 g	-	1.0 g	-	-	0.1 g	0.4 g	0.2 g
CS-H:HTC	-	-	2.0 g	1.0 g	-	-	0.1 g	0.4 g	0.2 g
CS-L:HTC-N	2.0 g	-	-	-	1.0 g	-	0.1 g	0.4 g	0.2 g
CS-M:HTC-N	-	2.0 g	-	-	1.0 g	-	0.1 g	0.4 g	0.2 g
CS-H:HTC-N	-	-	2.0 g	-	1.0 g	-	0.1 g	0.4 g	0.2 g
CS-L:HTC-N-SA	2.0 g	-	-	-	-	1.0 g	-	0.4 g	0.2 g
CS-M:HTC-N-SA	-	2.0 g	-	-	-	1.0 g	-	0.4 g	0.2 g
CS-H:HTC-N-SA	-	-	2.0 g	-	-	1.0 g	-	0.4 g	0.2 g

CS-L: low molecular weight chitosan; CS-M: medium molecular weight chitosan; CS-H: high molecular weight chitosan; HTC: hydroxalcalite; HTC-N: nanoparticulate hydroxalcalite; HTC-N-SA: nanoparticulate hydroxalcalite interspersed with sodium alendronate; SA: sodium alendronate.

or dynamic swelling index was determined by immersing the membranes in phosphate buffer at a pH of 7.4. All tests were performed in triplicate with weighing after 3 hours of immersion and for immersion times of 24, 48, and 72 hours (adapted from Kuo *et al.*, 2009). Membranes that collapsed, tore, or disintegrated during the test did not have their percentage water absorption index calculated. The water absorption index of the membranes was determined from the following equation:

$$A (\%) = [(W2 - W1) / W1] \times 100,$$

where  $A$  (%) is the index of water absorption;  $W1$  is the initial weight of the dry membrane;  $W2$  is the wet membrane weight after immersion in phosphate buffer.

The mechanical properties of the membranes were assessed by a tensile strength test using a rectangular specimen, according to the standardized method for mechanical-dynamic tests defined by ASTM D882-02 (ASTM International, 2002), in universal equipment for mechanical tensile tests, microprocessed electromechanical compression and flexion Emic DL 2000 (Emic, Brazil).

The tensile strength was measured at room temperature for dry membrane fragments cut to an approximate size of  $1 \times 13$  mm, fixed in parallel claws, and subjected to tension under a 50 N load cell, at a constant displacement speed of 1.0 mm/minute, until the complete rupture of the membrane. Eighteen replicates were performed for each membrane (Adapted from Ojagh *et al.*, 2010). The tensile strength was determined using the following equation:

$$TS = F/A,$$

where TS (MPa) is the tensile strength;  $F$  (N) is the force required for the rupture of the membrane, and  $A$  ( $\text{mm}^2$ ) is the area of the membrane at the point of rupture (Ojagh *et al.*, 2010).

#### ***In vitro* assessment of cell viability and osteoinduction potential of membranes**

The cytotoxicity was evaluated on human osteoblasts (Saos-2 from the Cell Bank of Rio de Janeiro, code 0217). Cells were cultured in Dulbecco's Modified Eagle's Medium-high glucose with L-glutamine (DMEM, Sigma-Aldrich D6429) supplemented with 10% fetal bovine serum and 1% penicillin/streptomycin solution (Sigma-Aldrich P4333) at 37°C and 5% carbon dioxide ( $\text{CO}_2$ ).

The culture medium was changed every 3 days, and cells were subcultivated at the confluence (Pautke *et al.*, 2004). The cytocompatibility test was adapted from Mao *et al.* (2003) and Park *et al.* (2002). Briefly, individual membranes ( $5 \times 5$  mm in size) were placed in the center of the wells in a 96-well culture plate. Next, cells were added at a density of 40,000 cells/ $\text{cm}^2$  and then incubated for 24 hours. Cells were observed and photographed in an optical microscope coupled to a digital camera (10 $\times$ ; Coleman N107), and a 3-(4,5-dimethylthiazol-2-yl)-2,5-diphenyltetrazolium bromide (MTT) viability assay was performed according to the method of Mosmann (1983) with minor modifications. MTT solution (125  $\mu\text{l}$ –0.5 mg/ml) was added and incubated for 3 hours. Next, dimethyl sulfoxide (DMSO) was added, and cell viability was measured by absorbance at 500 nm using a microplate reader (TP-Reader, Thermoplate, Brazil). All readings were discounted of pure DMSO absorbance (approximately 0.25–0.30). Experiments were conducted in triplicate, and all data were expressed as means

$\pm$  standard deviation. The cell growth (%) of the test group was calculated based on absorbance (Abs) in relation to the control group using the following equation:

$$\text{Cell growth (\%)} = \frac{[\text{Abs}] \text{ Test group 24 hours}}{[\text{Abs}] \text{ Control group 24 hours}} \times 100.$$

#### **Profilometry assessment**

The surface morphology of the membranes was assessed by profilometry analysis using a noncontact optical profilometer, Nanovea 3D PS50 (California, USA), equipped with a chromatic confocal sensor, where the topographic roughness parameters were determined by measuring the linear surface roughness and the three-dimensional roughness. Membrane fragments ( $5 \times 5$  mm) were assessed in a scanning area and step of  $1 \times 1$  mm for linear surface roughness and 3  $\mu\text{m}$  for three-dimensional roughness, measuring three height profiles for both faces of each membrane, with all experiments performed in triplicate.

#### ***In vitro* release assay**

The *in vitro* release profile was accessed through a dialysis bag method (Valle *et al.*, 2019). Briefly, the membrane was added to a dialysis bag (cellulose acetate; 1.3 kDa cutoff; Sigma-Aldrich, St. Louis, MO) and inserted into a Becker containing 100 ml of purified water ( $n = 3$ ). The system was incubated at 37°C under constant stirring. Samples (2 ml) were withdrawn at predetermined time intervals (2, 4, 16, 20, and 24 hours) and quantified.

Sodium alendronate quantification was performed on a Shimadzu high performance liquid chromatography equipped with Pump LC 20AT, Autosampler SIL 20A, Column Oven CTO10A, and Knauer RI Detector 2300, Smartline. The chromatographic column was a Waters IC-PAK Anion HC ( $4.6 \times 150$  mm, 10  $\mu\text{m}$ ). The chromatographic conditions followed the methodology described by Krishna *et al.* (2015). The linearity of the method was established in the range of 75–950  $\mu\text{g/ml}$ , and the selectivity was evaluated against the standard (alendronate sodium in mobile phase), blank (membrane without sodium alendronate in mobile phase), and contaminated blank (membrane without sodium alendronate in mobile phase contaminated with sodium alendronate).

#### **Statistical analysis**

All results were calculated and statistically assessed using SigmaPlot® software, version 12.5, Systat Software. One-way analysis of variance was used to comparatively assess results, and a  $p$ -value less than 0.05 was considered statistically significant. Saos-2 cell proliferation results were statistically evaluated using the Holm–Sidak method, which was used for all pairwise multiple comparison procedures, and the overall significance level was 0.05.

## **RESULTS AND DISCUSSION**

### **Preparation and characterization of nanoparticulate hydroxycalcite and nanoparticulate hydroxycalcite interspersed with sodium alendronate**

The samples of nanoparticulate hydroxycalcite after nanomilling presented a reduction in the hydrodynamic diameter from  $700.6 \pm 15.8$  nm to  $578.6 \pm 78.2$  nm. Despite the slight



reduction in diameter, there was also a reduction in the PDI value from 0.233 to 0.200, indicating greater homogeneity in the size distribution after nanomilling. Figure 1 shows the diffractograms of hydrotalcite and nanoparticulate hydrotalcite, which are in accordance with standards described in mineralogy manuals (Allman and Jepsen, 1969). The maintenance of the  $2\theta$  reflection angles on nanoparticulate hydrotalcite reveals that the nanomilling process preserved the hydrotalcites structure for subsequent interlayering processes. The  $2\theta$  angles' values of hydrotalcite, as well as the corresponding interlayer distance for each angle, as described in the literature and experimentally determined, are presented in Table 2. The milling process of this silicate using a dry ball mill has not been described in the literature so far, and it is possible to use the obtained material as a nanocharge in different processes related to the preparation of nanocomposites.

The nanoparticulate hydrotalcite or nanoparticulate hydrotalcite interspersed with sodium alendronate was directly used to prepare membranes by interlayering with chitosan. In X-ray diffraction analysis, nanoparticulate hydrotalcite presents two reflection angles characteristic of hydrotalcite,  $11.42^\circ$  and  $23.14^\circ$ , corresponding to interlayer spacings of 7.75 and 3.84 Å, while for nanoparticulate hydrotalcite interspersed with sodium alendronate samples, the characteristic reflection angles disappear and a new reflection angle appears in the  $7^\circ$  region, corresponding to an interlayer spacing of 12 Å (Table 2). The increase in the interlayer spacing of hydrotalcite is suggestive of the previous alendronate anion interlayering between its lamellae in place of the carbonate anion released as  $\text{CO}_2$ . Several studies with different drugs interspersed in hydrotalcite reveal an increase in interlamellar distance after interlayering, thus corroborating

the hypothesis that the interlayering of sodium alendronate in hydrotalcite was successful in the present work (Allou *et al.*, 2017; Berber *et al.*, 2010; Costantino *et al.*, 2008, 2012; Milani *et al.*, 2013; Silion *et al.*, 2010).

Sodium alendronate is soluble in water, while hydrotalcite is insoluble in water. When the alendronate anion is interlayered between the lamellae of hydrotalcite, displacing the carbonate anion (released as  $\text{CO}_2$ ), the dry residue resulting from the supernatant (from four washing cycles) refers to the noninterlayered sodium alendronate, and then the amount of interlayered sodium alendronate can be determined by gravimetric analysis. The percentage of sodium alendronate interspersed in hydrotalcite was  $86.41\% \pm 0.22\%$ , calculated indirectly by assessing the dry residue mass resulting from the supernatant freeze-drying from the interlayering reaction. The dry residue obtained from freeze-dried precipitate was analyzed by infrared spectroscopy with Fourier transform (Fig. 2). The highlighted vibrational bands seem to confirm the identity of sodium alendronate in the material resulting from the interlayering reaction. The principal peaks at 961, 995, and  $1,066\text{ cm}^{-1}$  characterized the stretching of P–O, P–C, and  $p = \text{O}$  groups, respectively, and the peak at  $1,559\text{ cm}^{-1}$  can be assigned to stretching vibrational of the C–N bond (Oz *et al.*, 2019; Silverstein *et al.*, 2014).

#### Obtention and characterization of the chitosan-based membranes

Low, medium, and high molecular weight chitosans were used in the preparation of the membranes with hydrotalcite (material as supplied, nanomilled, and interspersed with sodium alendronate) to assess possible differences in performance depending on the molar mass of the polymer and with the purpose of the combination of those biomaterials to obtain organic composites that simulate the bone structure for guided bone regeneration.

All membranes showed good flexibility and manipulation, besides the absence of a shape memory effect. Initial tests using Labrasol® (PEG-8 glycol caprylate obtained from Gattefossé, Saint-Priest, France) as a plasticizer were performed, but unlike the good results for chitosan and sodium montmorillonite membranes reported by Villaça *et al.* (2017), the membranes obtained in this work using Labrasol® were very friable and not very flexible, which led to the adoption of triacetin (obtained from Multichemie, Cotia, São Paulo) as a plasticizer. The incorporation of triacetin, such as a plasticizer, into the membrane, improved these inherent limitations imparting flexibility and toughness and decreasing the glass transition temperature as observed following.

In the analysis of membranes by X-ray diffraction (Fig. 3), there is a clear change in the diffractogram profile in relation to nanoparticulate hydrotalcite with dispersed sodium alendronate (Fig. 3b) and nanoparticulate hydrotalcite interspersed with sodium alendronate (Fig. 3c). In the diffractograms of the membranes prepared with nanoparticulate hydrotalcite, an absence of the  $2\theta$  reflection angles characteristic of hydrotalcite is observed, with the disappearance of the  $2\theta$  reflection angle around the  $7^\circ$  region, characterizing the formation of exfoliated nanocomposites. When hydrotalcite, as supplied, was used (Fig. 3a), the diffraction profile remained practically unchanged, with indications of interlayering only with low molecular weight chitosan.

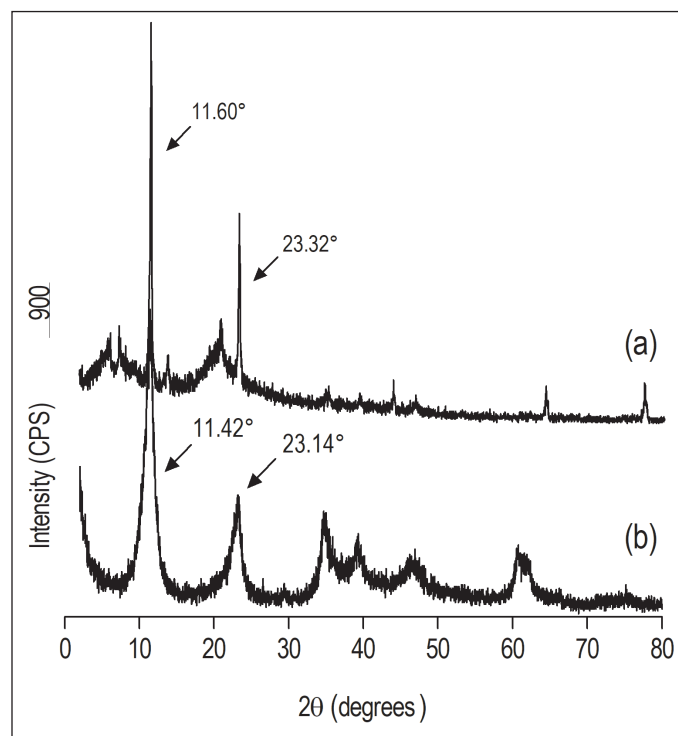


**Figure 1.** X-ray diffractograms of the (a) hydrotalcite as supplied and (b) nanoparticulate hydrotalcite.

**Table 2.** The  $2\theta$  angles values and the corresponding interlayer distance for each angle for the hydrotalcite standard according to literature, hydrotalcite as supplied, nanoparticulate hydrotalcite, and nanoparticulate hydrotalcite interspersed with sodium alendronate.

Sample	$2\theta$ ( $^\circ$ )	Interlayer distance ( $\text{\AA}$ )
Hydrotalcite standard <sup>a</sup>	11.64/23.40	7.60/3.80
Hydrotalcite as supplied	11.60/23.32	7.62/3.81
Nanoparticulate hydrotalcite	11.42/23.14	7.75/3.84
Nanoparticulate hydrotalcite interspersed with sodium alendronate	$7.11 \pm 0.06^b$	$12.43 \pm 0.11^b$

<sup>a</sup>Allman and Jepsen (1969).

<sup>b</sup>Mean  $\pm$  standard deviation.

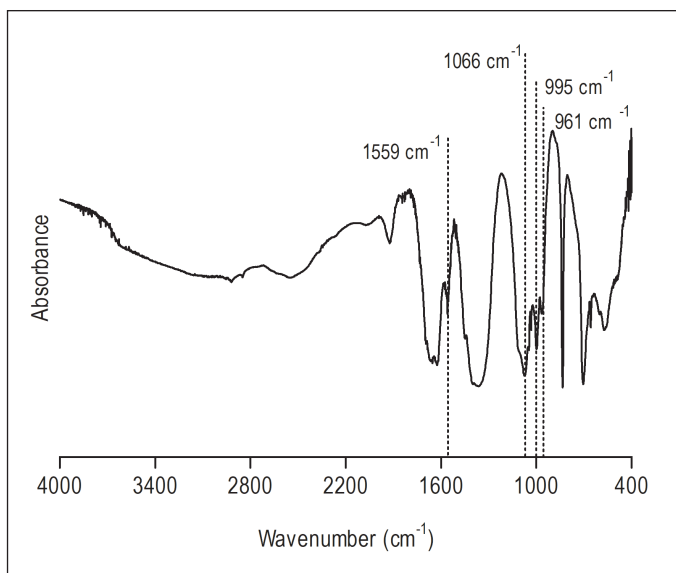


**Figure 2.** Fourier transform infrared spectroscopy spectrum of the nanoparticulate hydrotalcite interspersed with sodium alendronate.

All membranes were analyzed by differential exploratory calorimetry (Fig. 4). Thermal events such as glass transition are important in the physical characterization of polymers such as chitosan, where the material changes from a glassy to an elastic state (Dong *et al.*, 2004), while the melting temperature is important in the characterization of crystalline materials such as sodium alendronate. All thermograms show an endothermic event in the range of 69°C to 93°C. According to Dong *et al.* (2004), the glass transition of dry chitosan is between 118°C and 150°C; however, as per Dhawade and Jagtap (2012), the glass transition of hydrated chitosan is reduced to the range of 61°C to 85°C because water acts as a plasticizer. The presence of other plasticizing liquids also causes a reduction in chitosan glass transition; thus, this endothermic event observed in the range of 69°C to 93°C can be attributed to the polymer glass transition.

Sodium alendronate melting can be observed as an endothermic event that occurs in the range of 233°C to 235°C, and the displacement of that event to higher temperatures, as observed in the nanoparticulate hydrotalcite with dispersed sodium alendronate series membranes (258.58°C–259.47°C), suggests the introduction of sodium alendronate in the nanocomposite. According to Krzaczkowska *et al.* (2010), displacements or disappearances of thermal events characteristic of pure substances

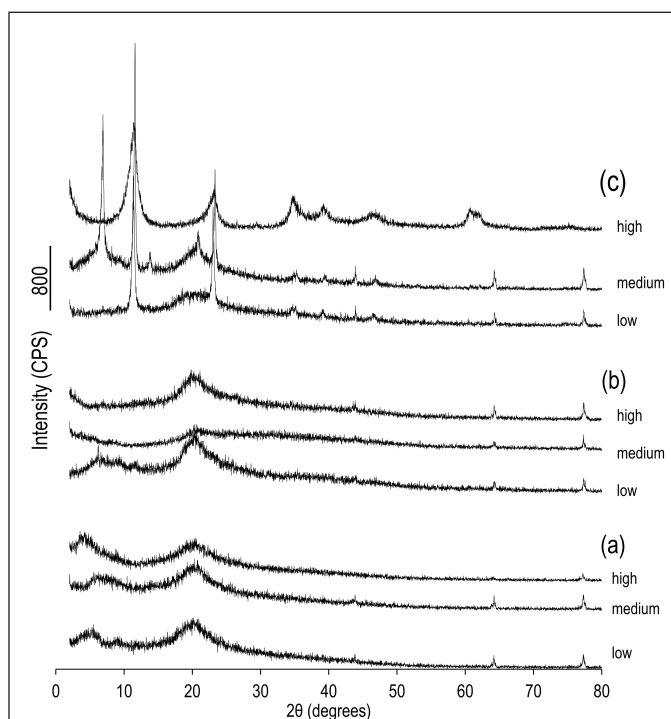


**Figure 3.** X-ray diffractograms of the chitosan-based membranes (low, medium, or high molecular weight chitosan) structured with (a) hydrotalcite as supplied with dispersed sodium alendronate; (b) nanoparticulate hydrotalcite with dispersed sodium alendronate; and (c) nanoparticulate hydrotalcite interspersed with sodium alendronate.

indicate strong interactions between the substance and the polymer, resulting in the formation of a nanocomposite. Therefore, the same behavior is expected for the nanoparticulate hydrotalcite interspersed with sodium alendronate membranes since the sodium alendronate is interlayered, that is, in strong interaction with the interlayer domain of the nanoparticulate hydrotalcite.

When placed in a liquid medium, the hydration capacity of a membrane by swelling and retention of a given water volume absorbed in its three-dimensional network is fundamental for its clinical applicability (Kuo *et al.*, 2009; Sager *et al.*, 2012) since they should absorb fluid from the body for cell transference, plus they should allow adequate distribution of nutrients, metabolites, and growth factors, through extracellular media (Rodríguez-Vázquez *et al.*, 2015). Moreover, the swelling of the polymer favors its bioadhesiveness, increasing the contact area of the membrane with the treated tissue (Fonseca-Santos *et al.*, 2017). On the

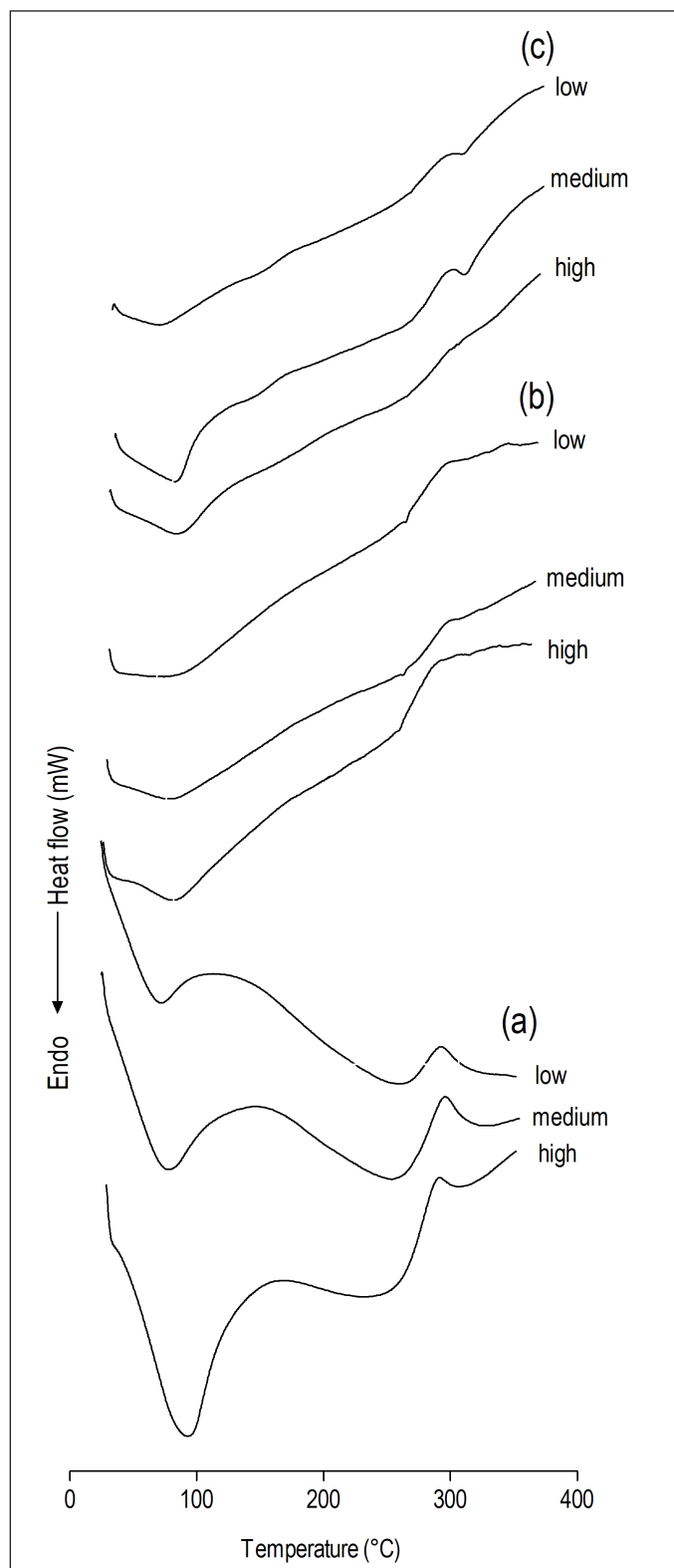


**Figure 4.** Differential scanning calorimetry thermograms obtained for chitosan-based membranes (low, medium, or high molecular weight chitosan) structured with (a) hydrothermalite as supplied; (b) nanoparticulate hydrothermalite with dispersed sodium alendronate; and (c) nanoparticulate hydrothermalite interspersed with sodium alendronate.

other hand, factors such as excessive water absorption affecting its integrity, or even the presence of inorganic material, making the membrane hydrophobic, can affect its clinical applicability

(Ojagh *et al.*, 2010). All membranes prepared with hydrothermalite as supplied collapsed within the first 80 minutes of the test. The high chitosan hydrophilicity, added to the weak interactions at the interface between the chitosan and the hydrothermalite as supplied particles, due to the absence of nanocomposite formation, possibly contributed to its rapid collapse. The results of dynamic water absorption for the nanoparticulate hydrothermalite with dispersed sodium alendronate and nanoparticulate hydrothermalite interspersed with sodium alendronate membranes are shown in Table 3.

The chitosan membranes prepared with nanoparticulate hydrothermalite with dispersed sodium alendronate withstood the 72 hours of testing, maintaining their integrity by absorbing less water (around 30%) than the chitosan and calcium phosphate membranes prepared by Kuo *et al.* (2009), while the membranes of chitosan with nanoparticulate hydrothermalite interspersed with sodium alendronate showed greater water absorption (about 55%), also resisting the 72 hours of testing. The good water absorption rates observed for membranes prepared with nanoparticulate hydrothermalite are probably due to the formation of a nanocomposite, whose interaction at the interface between chitosan and nanoparticulate hydrothermalite produced an increase in the resistance of the material, sufficient to keep the membranes intact until the end of the test.

In guided bone regeneration, membranes must have adequate mechanical properties to support the growth of bone tissue and be able to support similar forces as the natural bone (Bhowmick *et al.*, 2018; Vyas *et al.*, 2017). Therefore, it is important to evaluate their mechanical properties. The tensile strength of the trabecular bone can reach values of up to 50 MPa, and its density and mechanical strength parameters have been widely explored as a model for developing new materials for guided bone regeneration (Furst *et al.*, 2016).

The tensile strength test was performed with all membranes that did not collapse in the dynamic water absorption test, and the results are shown in Table 3. The experimental values obtained for the nanoparticulate hydrothermalite membranes were between 25.38% ( $37.31 \pm 3.13$  MPa) and 70.7% ( $14.65 \pm 4.79$  MPa), both below the tensile strength that the trabecular bone can reach (50 MPa). Despite this, the tensile strength values for developed membranes were equivalent to or greater than those reported for other biomaterials, such as sintered porous hydroxyapatite implants ( $17.4 \pm 0.3$  MPa) (Dong *et al.*, 2001) and chitosan microsphere ( $14.78 \pm 0.67$  MPa) (Meng *et al.*, 2015). In comparison, the membranes developed in this study showed significantly higher tensile strength than pure chitosan membranes ( $9.5 \pm 1.5$  MPa) and also than the commercial collagen membrane Bio-Guide® used in clinical practice for guided bone regeneration, whose tensile strength values are quite low ( $1.38 \pm 0.9$  MPa) (Vilaça *et al.*, 2017). In the sodium alendronate dispersed membranes, high molecular weight chitosan gave the largest strength, but the same correlation cannot be observed for the membranes interspersed with sodium alendronate. Although the same mass of solids was used in all prepared membranes, a difference in thickness among the evaluated membranes was observed. Zare and Garmabi (2015) mentioned that the thickness of the membrane is an important factor capable of altering its tensile strength. The average thickness of the membranes developed in this study was  $120.0 \pm 70.0$   $\mu\text{m}$ , thus assuming the impact on tensile strength and possibly further improving the tensile strength value of the developed membranes by increasing their thickness.

**Table 3.** Tensile strength test results and dynamic water absorption for membranes.

Membrane code	Description	Tensile strength (MPa)	Water absorption (%)
CS-L:HTC-N		14.65 ± 4.79 <sup>a*</sup>	31.11 ± 4.73 <sup>*</sup>
CS-M:HTC-N	Sodium alendronate dispersed	18.85 ± 1.82 <sup>a*</sup>	34.39 ± 1.93 <sup>**</sup>
CS-H:HTC-N		31.70 ± 5.91 <sup>a***</sup>	34.02 ± 1.28
CS-L:HTC-N-SA		37.31 ± 3.13 <sup>a****</sup>	58.25 ± 0.98 <sup>*</sup>
CS-M:HTC-N-SA	Interspersed with sodium alendronate	18.95 ± 3.09 <sup>a*</sup>	54.60 ± 10.61
CS-H:HTC-N-SA		21.61 ± 2.15 <sup>a*</sup>	66.77 ± 0.42
Chitosan membrane	Other	9.50 ± 1.50 <sup>b</sup>	-
Bio-Guide®		1.38 ± 0.90 <sup>b</sup>	-

\*  $p > 0.05$ .\*\*  $p < 0.005$ .\*\*\*  $p < 0.001$ .\*\*\*\*  $p < 0.0001$ .<sup>a</sup> Mean values obtained in multiple and independent tests with  $n = 18$ .<sup>b</sup> Mean values obtained by Villaça *et al.* (2017) in multiple and independent tests with  $n = 7$ , performed under the same experimental conditions and equipment.

Mean ± standard deviation.

### ***In vitro* assessment of Saos-2 cells line viability and osteoinduction potential of membranes**

Biocompatibility is a primordial characteristic that a membrane suitable for guided bone regeneration needs to present, and for that, it must be assessed against human bone cells (Bhowmick *et al.*, 2018). The osteoblastic properties of Saos-2 human osteosarcoma cells were characterized by Rodan *et al.* (1987), confirming that such cells have a mature osteoblast phenotype, with high levels of phosphatase alkaline and cell spindle morphology, which are considered markers for osteoblastic cell differentiation (Ayobian-Markazi *et al.*, 2015; Rodan *et al.*, 1987).

All developed nanocomposite membranes, as well as their physical mixtures and pure chitosan membranes with low, medium, and high molecular weight, were analyzed using a cell culture medium (DMEM) as a negative control. Images obtained by optical microscopy demonstrating the effect of samples on cell growth at 24 hours are shown in Figure 5. After 24 hours, a high density of adhered spindle-shaped cells was observed, denoting possible cell differentiation with only small empty spaces between cells. It was impossible to establish a direct correlation between the images and osteoinduction potential; thus, it was necessary to quantitatively assess cell proliferation by the MTT test, whose results are presented in Figure 6.

It is noteworthy that all groups of samples had a higher proliferation rate ( $p < 0.001$ ) of Saos-2 cells than that in the negative control group, the most prominent being the nanoparticulate hydroxylapatite with dispersed sodium alendronate membranes (membranes 2–4 in Fig. 6). Membrane 3 showed higher cell proliferation ( $p < 0.005$ ) than all the other groups, except for membrane 2, which showed no statistically significant difference compared to membrane 3. Membranes prepared from the physical mixture (membranes 8–10) exhibited inferior behavior to nanoparticulate hydroxylapatite with dispersed sodium alendronate membrane series, mainly 2 and 3 membranes ( $p < 0.005$ ). However, the main difference between these membrane series (2–4 vs. 8–10) is the stirring time during processing. So, it seems that the stirring time is the limiting factor for attaining the state of homogeneity of the components, interlayering of the

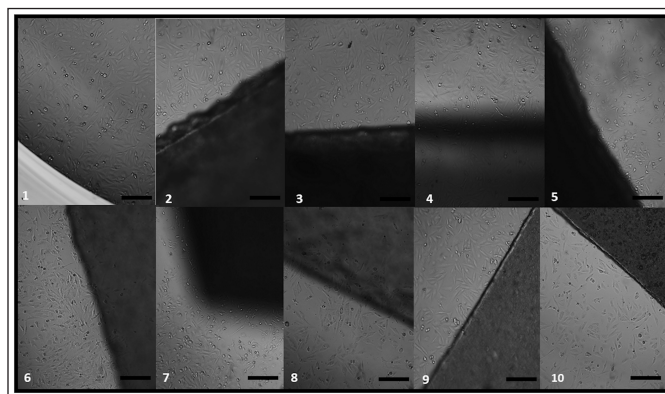


**Figure 5.** Images obtained by optical microscopy Saos-2 cells at the border of membranes. Samples: (1) Medium control; chitosan-based membranes series structured with nanoparticulate hydroxylapatite with dispersed sodium alendronate containing low (2), medium (3), or high (4) molecular weight chitosan; chitosan-based membranes series structured with nanoparticulate hydroxylapatite interspersed with sodium alendronate containing low (5), medium (6), or high (7) molecular weight chitosan; the physical mixture of the nanoparticulate hydroxylapatite interspersed with sodium alendronate with low (8), medium (9), or high (10) molecular weight chitosan. Optical microscopy image at 200  $\mu\text{m}$  scale bar.

nanocomposite, and structuring of the membrane provided by the additional process energy.

The membranes of the nanoparticulate hydroxylapatite interspersed with sodium alendronate series (5–7) showed cell growth rates for 24 hours lower than those of the nanoparticulate hydroxylapatite with dispersed sodium alendronate series (2–4). A possible explanation for its lower performance in relation to the nanoparticulate hydroxylapatite with dispersed sodium alendronate membranes is that the sodium alendronate is interspersed in nanoparticle hydroxylapatite of these membranes, and it is not fully available as it was for membranes with dispersed sodium alendronate. This would not necessarily anticipate a negative *in vivo* performance, where enzymatic degradation pathways could release the drug on its target and clinical use would last months. Thus, nanoparticulate hydroxylapatite interspersed with sodium



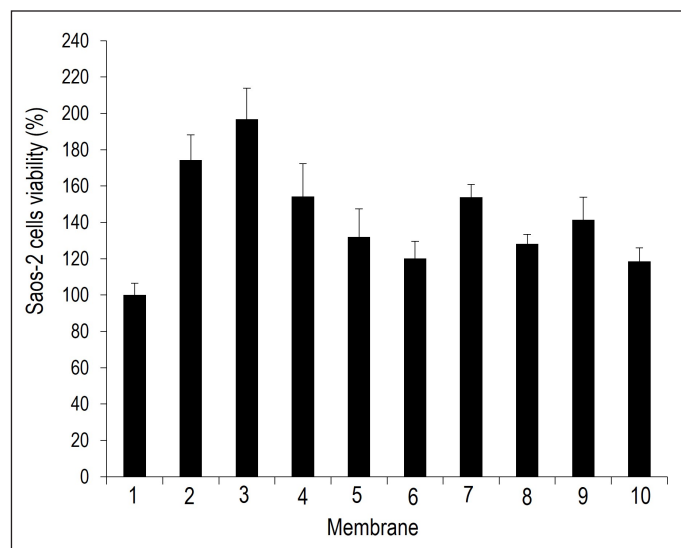


**Figure 6.** Saos-2 cell viability results after exposure to membranes. Samples: (1) medium control; chitosan-based membranes series structured with nanoparticulate hydroxylapatite with dispersed sodium alendronate containing low (2), medium (3), or high (4) molecular weight chitosan; chitosan-based membranes series structured with nanoparticulate hydroxylapatite interspersed with sodium alendronate containing low (5), medium (6), or high (7) molecular weight chitosan; the physical mixture of the nanoparticulate hydroxylapatite interspersed with sodium alendronate with low (8), medium (9), or high (10) molecular weight chitosan. The error bars represent the standard deviation between the measurements for each group.

alendronate membranes could act as a sodium alendronate-controlled release system *in vivo*, but further experiments would be necessary to confirm this hypothesis. However, the lowest cell growth rates for this membrane series (2–4) may not be related to the membrane itself but to time (hours to a few days) limitations of the assay for the drug release compared to the time of clinical use of the membrane in guided bone regeneration therapy (around 4–6 months).

The biomaterial structure produced is an important parameter for cell adhesion, material degradation, and replacement by functional tissue. The chitosan used for the production of the membranes in this study differs in molecular weight but exhibits the same deacetylation degree (75%–85%). Abarrategi *et al.* (2010) reported a considerable influence of molecular weight, ranging from laminated scaffolds for high molecular weight to fibrillar with much more open structures for low molecular weight. Results suggest that low molecular weight forms a nanocomposite with a more favorable structure for cell interaction and colonization (Abarrategi *et al.*, 2010), besides acting as a promoter of the activation of genes that are responsible for the expression of proteins that directly affect osteoblastic cell proliferation (Ohara *et al.*, 2004).

Both formations of new nanocomposite with intrinsic properties offered by chitosan and hydroxylapatite and the presence of sodium alendronate must be observed to obtain a positive result for membranes. Thus, the trials revealed that the combination of chitosan, hydroxylapatite, and sodium alendronate showed biocompatibility and a positive bias for cell adhesion, proliferation, and possible differentiation *in vitro* and the absence of toxicity to Saos-2 cells. Considering the limitations of the assay,

results suggest that the best membranes were those obtained with sodium alendronate dispersed in nanoparticulate hydroxylapatite, notably for low and medium chitosan molecular weights (2 and 3, respectively).

### Profilometry assessment

The membrane surface roughness is an important parameter to facilitate cell adhesion, proliferation, and differentiation in the bone regeneration process. Thus, only the membrane and its physical mixture, which showed the best performance in the *in vitro* assessment of cell viability and osteoinduction potential, had their linear roughness assessed by profilometry. The linear roughness parameter ( $\mu\text{m}$ ) represented average surface roughness and was determined on both sides of the chitosan-based hydroxylapatite nanostructured membrane (CS-L:HTC-N) with dispersed sodium alendronate. The results showed that the membrane had linear roughness of  $4.49 \pm 0.08 \mu\text{m}$  (smooth side) and  $4.35 \pm 0.03 \mu\text{m}$  (rough side) and was significantly higher than a pure chitosan membrane ( $0.40 \pm 0.10 \mu\text{m}$ ) described by Villaça *et al.* (2017). The profilometry assessment was performed under the same experimental conditions and equipment.

The linear roughness shown by CS-L:HTC-N with dispersed sodium alendronate indicates that it can be used as structural support in bone regeneration since it can promote proper cell proliferation in the action site and also have enough surface area for live cells to accommodate adequately.

### *In vitro* release assay

The scientific literature describes several methodologies for the quantification of sodium alendronate, usually involving derivatization with reagents such as o-phthalaldehyde (Al Deeb *et al.*, 2004) and ninhydrin reagent in the presence of pyridine (Alarfaj *et al.*, 2011) for fluorescence or ultraviolet detection. In addition, ion exchange chromatography with a refractive index detector was reported (Krishna *et al.*, 2015). The three techniques above were tested, but the selectivity was only observed with the refractive index detector, and therefore, this technique was chosen for the quantification of sodium alendronate. The method was linear in the range of 75–950  $\mu\text{g/ml}$  ( $y = 28.943 \times - 825.9$ ,  $R^2 = 0.998$ ).

As expected, *in vitro* release of alendronate dispersed in the CS-L:HTC-N was not observed. However, it is expected that alendronate will be released from the membrane by enzymatic action *in vivo* at the site of action in the space between the gum and tooth created as a result of periodontal surgical procedures. The degradation behavior of chitosan plays a crucial role in the long-term performance of a chitosan membrane. Many reports on the degradation of chitosan by chitotriosidase, for example, show that the degree of N-deacetylation of chitosan is one of the key factors controlling the degradation behavior of chitosan (Zainol *et al.*, 2009; Eide *et al.*, 2012). Also, there is the time (hours) limitation of the assay for sodium alendronate release compared to the estimated time of clinical use of the membrane in guided bone regeneration therapy, which is 4 to 6 months.

### CONCLUSION

It was possible to obtain nanoparticulate hydroxylapatite by a dry nanomilling process not yet described in the literature by obtaining particles on the nanometer scale and with a reflection

profile similar to that observed in the starting material (hydrotalcite as supplied), showing that the proposed nanomilling method did not change the crystallographic structure of hydrotalcite. The preparation of chitosan-based hydrotalcite nanoparticulate structures interspersed with sodium alendronate or with dispersed sodium alendronate led to a change in the reflection profile with an increase in the interlayer distance of hydrotalcite, indicating the achievement of an exfoliated nanocomposite, with its good yield confirmed by gravimetric analysis and infrared spectroscopy of the freeze-dried residue from the supernatant after centrifugation. Chitosan membranes obtained with nanoparticulate hydrotalcite with dispersed sodium alendronate and nanoparticulate hydrotalcite interspersed with sodium alendronate showed good results in the dynamic water absorption test and the tensile strength test, and all membranes that were subjected to *in vitro* assessment of cell viability and osteoinduction potential showed biocompatibility. The nanoparticulate hydrotalcite with dispersed sodium alendronate membrane series showed better performance in the *in vitro* test, but *in vivo* tests must be performed to investigate the clinical aspects of such membranes.

#### ACKNOWLEDGMENTS

This work was supported by Fundação Carlos Chagas Filho de Amparo à Pesquisa do Estado do Rio de Janeiro (FAPERJ), Conselho Nacional de Desenvolvimento Científico e Tecnológico (CNPq), and Coordenação de Aperfeiçoamento de Pessoal de Nível Superior (CAPES).

#### AUTHOR CONTRIBUTIONS

**FLCS** was responsible for the conceptualization, formal analysis, investigation, methodology, and writing of the original draft. **AS** contributed to the investigation, methodology, writing of the original draft, and the review and editing of the article. **ELBD, RFS, and APMC** were responsible for formal analysis and methodology. **CRR** contributed to methodology, funding acquisition, and resources. **LCRPS** was responsible for the formal analysis, investigation, methodology, and writing of the original draft. **FAC** contributed to the investigation, methodology, writing of the original draft, and the review and editing of the article. **LMC** was responsible for the conceptualization, data curation, funding acquisition, project administration, resources, supervision, writing of the original draft, and the review and editing of the article.

#### CONFLICTS INTERESTS

The authors declare that they have no competing financial interests or personal relationships that could have appeared to influence the work reported in this article.

#### ETHICAL APPROVALS

This study does not involve experiments on animals or human subjects.

#### DATA AVAILABILITY

All data generated and analyzed are included in this research article.

#### PUBLISHER'S NOTE

This journal remains neutral with regard to jurisdictional claims in published institutional affiliation.

#### REFERENCES

- Abarrategi A, Lópiz-Morales Y, Ramos V, Civantos A, López-Duñ L, Marco F, López-Lacomba JL. Chitosan scaffolds for osteochondral tissue regeneration. *J Biomed Mater Res Part A*, 2010; 95(4):1132–41.
- Alarfaj NA, El-Razeq SAA, Al-Qahtani FN. Spectrophotometric determination of alendronate sodium in bulk drug and in pharmaceutical formulation. *Asian J Chem*, 2011; 23(2):697–700.
- Al Deeb SK Hamdan, II Al Najjar SM. Spectroscopic and HPLC methods for the determination of alendronate in tablets and urine. *Talanta*, 2004; 64(3):695–702.
- Allman R, Jepsen HP. Die struktur des hydrotalkits. *Neues Jahrb für Mineral Monatsh*, 1969; 1969:544–51.
- Allou NB, Saikia P, Borah A, Goswamee RL. Hybrid nanocomposites of layered double hydroxides: an update of their biological applications and future prospects. *Colloid Polym Sci*, 2017; 295(5):725–47.
- Ambrogio V, Fardella G, Grandolini G, Perioli L, Tiralti MC. Intercalation compounds of hydrotalcite-like anionic clays with anti-inflammatory agents, II: uptake of diclofenac for a controlled release formulation. *AAPS Pharm Sci Tech*, 2002; 3(3):77–82.
- ASTM International. ASTM D882: standard test method for tensile properties of thin plastic sheeting. ASTM International, Pennsylvania, PA, 2002.
- Ayobian-Markazi N, Karimi M, Safar-Hajhosseini A. Effects of Er: YAG laser irradiation on wettability, surface roughness, and biocompatibility of SLA titanium surfaces: an *in vitro* study. *Lasers Med Sci*, 2015; 30(2):561–66.
- Basile MA, D'Ayala GG, Malinconico M, Laurienzo P, Coudane J, Nottelet B, Ragione FD, Oliva A. Functionalized PCL/HA nanocomposites as microporous membranes for bone regeneration. *Mater Sci Eng C Mater Biol Appl*, 2015; 48:457–68.
- Berber MR, Hafez IH, Minagawa K, Mori T, Tanaka M. Nanocomposite formulation system of lipid-regulating drugs based on layered double hydroxide: Synthesis, characterization and drug release properties. *Pharm Res*, 2010; 27(11):2394–401.
- Betz RR. Limitations of autograft and allograft: new synthetic solutions. *Orthopedics*. 2002; 25(5):561–70.
- Bhowmick A, Banerjee SL, Pramanik N, Jana P, Mitra T, Gnanamani A, Das M, Kundu PP. Organically modified clay supported chitosan/hydroxyapatite-zinc oxide nanocomposites with enhanced mechanical and biological properties for the application in bone tissue engineering. *Int J Biol Macromol*, 2018; 106:11–9.
- Boanini E, Torricelli P, Gazzano M, Giardino R, Bigi A. Alendronate-hydroxyapatite nanocomposites and their interaction with osteoclasts and osteoblast-like cells. *Biomaterials*, 2008; 29(7):790–6.
- Cao L, Yu Y, Wang J, Werkmeister JA, McLean KM, Liu C. 2-N, 6-O-sulfated chitosan-assisted BMP-2 immobilization of PCL scaffolds for enhanced osteoinduction. *Mater Sci Eng C Mater Biol Appl*, 2017; 74:298–306.
- Coelho ACVC, Santos PS. Argilas especiais: argilas químicas modificadas—uma revisão. *Quím Nova*, 2007; 30(5):1282–94.
- Costantino U, Ambrogio V, Nocchetti M, Perioli L. Hydrotalcite-like compounds: versatile layered hosts of molecular anions with biological activity. *Microporous Mesoporous Mater*, 2008; 107(1–2):149–60.
- Costantino U, Nocchetti M, Tammaro L, Vittoria V. Modified hydrotalcite-like compounds as active fillers of biodegradable polymers for drug release and food packaging applications. *Recent Pat Nanotechnol*, 2012; 6(3):218–30.
- Dahlin C, Sennerby L, Lekholm U, Linde A, Nyman S. Generation of new bone around titanium implants using a membrane technique: an experimental study in rabbits. *Int J Oral Maxillofac Implants*, 1989; 4(1):19–25.
- Dhawade PP, Jagtap RN. Characterization of the glass transition temperature of chitosan and its oligomers by temperature modulated differential scanning calorimetry. *Pelagia Res Lib Adv Appl Sci Res*, 2012; 3(3):1372–82.
- Dong J, Uemura T, Kikuchi M, Tateishi T, Tanaka J. *In vivo* evaluation of a novel porous hydroxyapatite to sustain osteogenesis of transplanted bone marrow-derived osteoblastic cells. *J Biomed Mater Res*, 2001; 57:208–16.

- Dong Y, Ruan Y, Wan H, Zhao Y, Bi D. Studies on glass transition temperature of chitosan with four techniques. *J Appl Polym Sci*, 2004; 93(4):1553–8.
- Eide KB, Norberg AL, Heggset EB, Lindbom AR, Vårum KM, Eijssink VGH, Sørli M. Human chitotriosidase-catalyzed hydrolysis of chitosan. *Biochem*, 2012; 511:487–95.
- Farraro KF, Kim KE, Woo SLY, Flowers JR, McCullough MB. Revolutionizing orthopaedic biomaterials: the potential of biodegradable and bioresorbable magnesium-based materials for functional tissue engineering. *J Biomech*, 2014; 47(9):1979–86.
- Fonseca-Santos B, Satake CY, Calixto GMF, Dos Santos AM, Chorilli M. Trans-resveratrol-loaded nonionic lamellar liquid-crystalline systems: structural, rheological, mechanical, textural, and bioadhesive characterization and evaluation of *in vivo* anti-inflammatory activity. *Int J Nanomed*, 2017; 12:6883–93.
- Furst JR, Bandeira LC, Fan WW, Agarwal S, Nishiyama KK, McMahon DJ, Dworakowski E, Jiang H, Silverberg SJ, Rubin MR. Advanced glycation endproducts and bone material strength in type 2 diabetes. *J Clin Endocrinol Metab*, 2016; 101(6):2502–10.
- Giannitelli SM, Basoli F, Mozetic P, Piva P, Bartuli FN, Luciani F, Arcuri C, Trombetta M, Rainer A, Licoccia S. Graded porous polyurethane foam: a potential scaffold for oro-maxillary bone regeneration. *Mater Sci Eng C*, 2015; 51:329–35.
- Herald E, Suprihatin RW, Pranoto. Intercalation of diclofenac in modified Zn/Al hydrotalcite-like preparation. *IOP Conf Ser Mater Sci Eng*, 2016; 107(1):012026.
- Huang B, Liu M, Zhou C. Chitosan composite hydrogels reinforced with natural clay nanotubes. *Carbohydr Polym*, 2017; 175(8):689–98.
- Kawase T, Yamanaka K, Suda Y, Kaneko T, Okuda K, Kogami H, Nakayama H, Nagata M, Wolff LF, Yoshie H. Collagen-coated poly(1-lactide-co-ε-caprolactone) film: a promising scaffold for cultured periosteal sheets. *J Periodontol*, 2010; 81(11):1653–62.
- Killeen AC, Rakes PA, Schmid MJ, Zhang Y, Narayana N, Marx DB, Payne JB, Wang D, Reinhardt RA. Impact of local and systemic alendronate on simvastatin-induced new bone around periodontal defects. *J Periodontol*, 2012; 83(12):1463–71.
- Kong Q, Wu T, Zhang H, Zhang Y, Zhang M, Si T, Yang L, Zhang J. Improving flame retardancy of IFR/PP composites through the synergistic effect of organic montmorillonite intercalation cobalt hydroxides modified by acidified chitosan. *Appl Clay Sci*, 2017; 146(2):230–7.
- Krishna MVNM, Rao SV, Venugopal NVS, Mantena BPV. *In vitro* dissolution method for alendronate sodium and vitamin D3 tablets using HPLC with combination of refractive index and ultraviolet detectors. *Anal Chem Lett*, 2015; 5(4):216–28.
- Krzaczekowska J, Strankowski M, Jurga S, Jurga K, Pietraszko A. NMR dispersion studies of poly(ethylene oxide)/sodium montmorillonite nanocomposites. *J Non-Cryst Solids*, 2010; 356(20–22):945–51.
- Kumar-Krishnan S, Prokhorov E, Hernández-Iturriaga M, Mota-Morales JD, Vázquez-Lepe M, Kovalenko Y, Sanchez IC, Luna-Bárceñas G. Chitosan/silver nanocomposites: synergistic antibacterial action of silver nanoparticles and silver ions. *Eur Polym J*, 2015; 67:242–51.
- Kuo SM, Chang SJ, Niu GCC, Lan CW, Cheng WT, Yang CZ. Crystallization behavior of poly(ε-caprolactone)/layered double hydroxide nanocomposites. *J Appl Polym Sci*, 2009; 116(5):2658–67.
- Lee SW, Kim SG. Membranes for the guided bone regeneration. *Maxillofac Plastic Reconstr Surg*, 2014; 36(6):239–46.
- Logithkumar R, Keshavnarayan A, Dhivya S, Chawla A, Saravanan S, Selvamurugan N. A review of chitosan and its derivatives in bone tissue engineering. *Carbohydr Polym*, 2016; 151:172–88.
- Mao JS, Liu HF, Yin, YJ, De Yao K. The properties of chitosan-gelatin membranes and scaffolds modified with hyaluronic acid by different methods. *Biomater*, 2003; 24(9):1621–9.
- Meng D, Dong L, Wen Y, Xie Q. Effects of adding resorbable chitosan microspheres to calcium phosphate cements for bone regeneration. *Mater Sci Eng C*, 2015; 47:266–72.
- Milani ME, Ponzi MI, Herrera P, Flores RC. Intercalación de Diclofenac Sódico en Compuestos tipo Hidrotalcitas. AAIQ, Asociación Argentina de Ingenieros Químicos—VII CIAQ Buenos Aires, Argentina., 2013.
- Mosmann, T. Rapid colorimetric assay for cellular growth and survival: application to proliferation and cytotoxicity assays. *J Immunol Methods*, 1983; 65:55–63.
- Ohara, N, Hayashi Y, Yamada S, Kim SK, Matsunaga T, Yanagiguchi K, Ikeda T. Early gene expression analyzed by cDNA microarray and RT-PCR in osteoblasts cultured with water-soluble and low molecular chitooligosaccharide. *Biomater*, 2004; 25(10):1749–54.
- Ojagh SM, Rezaei M, Razavi SH, Hosseini SMH. Development and evaluation of a novel biodegradable film made from chitosan and cinnamon essential oil with low affinity toward water. *Food Chem*, 2010; 122(1):161–6.
- Oz UC, Küçüktürkmen B, Devrim B, Saka OM, Bozkir A. Development and optimization of alendronate sodium loaded PLGA nanoparticles by central composite design. *Macromol Res*, 2019; 27(9):857–66.
- Park SN, Park JC, Kim HO, Song MJ, Suh H. Characterization of porous collagen/hyaluronic acid scaffold modified by 1-ethyl-3-(3-dimethylaminopropyl) carbodiimide cross-linking. *Biomater*, 2002; 23(4):1205–12.
- Parvini P, Obreja K, Sader R, Becker J, Schwarz F, Salti L. Surgical options in orofacial fistula management: a narrative review. *Int J Implant Dent* 2018; 274(1):40.
- Pautke C, Schieker M, Tischer T, Kolk A, Neth P, Mutschler W, Milz S. Characterization of osteosarcoma cell lines MG-63, Saos-2 and U-2 OS in comparison to human osteoblasts. *Anticancer Res*, 2004; 24(6):3743–8.
- Pradeep AR, Kumari M, Rao NS, Naik SB. 1% Alendronate gel as local drug delivery in the treatment of class II furcation defects: a randomized controlled clinical trial. *J Periodontol*, 2013; 84(3):307–15.
- Ren K, Wang Y, Sun T, Yue W, Zhang H. Electrospun PCL/gelatin composite nanofiber structures for effective guided bone regeneration membranes. *Mater Sci Eng C*, 2017; 78:324–32.
- Rodan SB, Imai Y, Thiede MA, Wesolowski G, Thompson D, Bar-Shavit Z, Shull S, Mann K, Rodan GA. Characterization of a human osteosarcoma cell line (Saos-2) with osteoblastic properties. *Cancer Res*, 1987; 47(18):4961–6.
- Rodríguez-Vázquez M, Vega-Ruiz B, Ramos-Zúñiga R, Saldaña-Koppel DA, Quiñones-Olvera LF. Chitosan and Its potential use as a scaffold for tissue engineering in regenerative medicine. *BioMed Res Int*, 2015:821279.
- Sager M, Ferrari D, Wieland M, Dard M, Becker J, Schwarz F. Immunohistochemical characterization of wound healing at two different bone graft substitutes. *Int J Oral Maxillofac Surg*, 2012; 41(5):657–66.
- Shahriarpanah S, Nourmohammadi J, Amoabediny G. Fabrication and characterization of carboxylated starch-chitosan bioactive scaffold for bone regeneration. *Int J Biol Macromol*, 2016; 93:1069–78.
- Sheikh Z, Khan AS, Roohpour N, Glogauer M, Rehman IU. Protein adsorption capability on polyurethane and modified-polyurethane membrane for periodontal guided tissue regeneration applications. *Mater Sci Eng C*, 2016; 68:267–75.
- Shokuhfar A, Zare-Shahabadi A, Atai AA, Ebrahimi-Nejad S, Termeh M. Predictive modeling of creep in polymer/layered silicate nanocomposites. *Polym Test*, 2012; 31(2):345–54.
- Silion M, Hritcu D, Jaba IM, Tamba B, Ionescu D, Mungiu OC, Popa IM. *In vitro* and *in vivo* behavior of ketoprofen intercalated into layered double hydroxides. *J Mater Sci Mater Med*, 2010; 21(11):3009–18.
- Silverstein RM, Webster FX, Kiemle DJ, Bryce DL. Spectrometric identification of organic compounds. 8th edition, Wiley, New York, NY, pp 1–464, 2014.
- Valle IV, Machado ME, Araújo CDCB, da Cunha-Junior EF, da Silva Pacheco J, Torres-Santos EC, da Silva LCRP, Cabral LM, do Carmo FA, Sathler PC. Oral pentamidine-loaded poly(D,L-lactic-co-glycolic) acid nanoparticles: an alternative approach for leishmaniasis treatment. *Nanotechnol*, 2019; 30:455102.
- Villaça JC, da Silva LC, de Alexandria AK, de Almeida GS, Locatelli FR, Maia LC, Rodrigues CR, de Sousa VP, Tavares MI, Cabral LM. Development and characterization of clay-polymer nanocomposite membranes containing sodium alendronate with osteogenic activity. *Appl Clay Sci*, 2017; 146:475–86.

Vyas V, Kaur T, Thirugnanam A. Chitosan composite three dimensional macroscopic scaffolds for bone tissue engineering. *Int J Biol Macromo*, 2017; 104:1946–54.

Wang CZ, Chen SM, Chen CH, Wang CK, Wang GJ, Chang JK, Ho ML. The effect of the local delivery of alendronate on human adipose-derived stem cell-based bone regeneration. *Biomater*, 2010; 31(33):8674–83.

Wang J, Wang L, Zhou Z, Lai H, Xu P, Liao L, Wei J. Biodegradable polymer membranes applied in guided bone/tissue regeneration: a review. *Polymers (Basel)*, 2016; 8(4):1–20.

Yun MH, Kwon KIL. High-performance liquid chromatography method for determining alendronate sodium in human plasma by detecting fluorescence: application to a pharmacokinetic study in humans. *J Pharm Biomed Anal*, 2006; 40(1):168–72.

Zainol I, Ghani SM, Mastor A, Derman MA, Yahya MF. Enzymatic degradation study of porous chitosan membrane. *Mater Res Innov*, 2009; (13)3:316–9.

Zare Y, Garmabi H. Thickness, modulus and strength of interphase in clay/polymer nanocomposites. *Appl Clay Sci*, 2015; 105106:66–70.

Zare Y, Rhee KY. Multistep modeling of Young's modulus in polymer/clay nanocomposites assuming the intercalation/exfoliation of clay layers and the interphase between polymer matrix and nanoparticles. *Compos Part A Appl Sci Manuf*, 2017; 102:137–44.

**How to cite this article:**

de Souza FLC, Simon A, D'Ornellas ELB, da Silva RF, Covas ACM, Rodrigues CR, da Silva LCRP, do Carmo FA, Cabral LM. Chitosan-based hydrotalcite nanostructured membranes containing sodium alendronate for guided bone regeneration therapy. *J Appl Pharm Sci*, 2023; 13(08):113–124.